MATDER

Comparative Study of Algebraic Wall Model and Differential Equation Wall Model in Large Eddy Simulation of Turbulent Channel Flow

Muhammad Saiful Islam Mallik[a,*], Mohammad Azizul Hoque[a,b], Md. Ashraf Uddin[b]

[a] Department of Arts and Sciences, Ahsanullah University of Science and Technology, Dhaka-1208, Bangladesh.
[b] Department of Mathematics, Shahjalal University of Science and Technology, Sylhet-3114, Bangladesh.

Abstract. A large eddy simulation (LES) is performed in a plane turbulent channel flow, where the near wall region is approximated by algebraic wall model (AWM) and differential equation wall model (DEWM). The simulation is performed by using a finite difference method of second order accuracy in space and a low-storage explicit Runge-Kutta method with third order accuracy in time. The computational results are compared with those from direct numerical simulation (DNS) data. Comparing the results throughout the calculation domain we have found that the results from the LES with DEWM (LES-DEWM) approach show closer agreement with the DNS results.

1. Introduction

The study on turbulent channel flow [5, 7, 13–15, 18, 21, 25, 30] is promising not only for understanding turbulence phenomena but also for testing of validation of turbulence models in numerical simulation. There are varieties of turbulence simulation technique, such as DNS [7, 16, 18], LES [2–5, 7, 14, 15, 19, 24, 25, 29, 30], RANS (Reynolds-averaged Navier-Stokes) and others. A simulation that resolves all the scales of turbulence motion is called DNS. But, due to its computational cost, still it is impractical for realistic engineering flows. On the other hand, RANS [6, 12] is the most used approximation to the solution of turbulent flow and this approach does not require large CPU resources. But one principal limitation of this approach is that the model used here must represent a very wide range of scales. An intermediate approach is the LES methodology. In LES, the computational cost is reduced by means of a filtering operation applied to the Navier-Stokes equations, thus eliminate many of the small scales below the filter width. This approach resolves explicitly the dynamics of the unsteady large scales of turbulence and models the smaller ones. Another approach in LES for the wall-bounded flows is to model the near-wall dynamics by wall stress models, e.g. Schumann model [21], Grötzbach model [7], Algebraic wall model [23], differential equation wall models [2–4, 27]. The main advantage of using such a model is that the resolution requirement for LES can be reduced significantly, thereby one can eliminate the computational cost much. Wall stress models supply wall shear stresses to the outer flow LES as a set of approximate boundary conditions. Another important issue for LES is the discretization method. A literature review suggests that for spatial discretization of the governing equations of LES the numerical methods

---

Corresponding Author

Email addresses: saiful.austmath@gmail.com (M.S.I. Mallik), azizmath.as@aust.edu (M.A. Hoque), auddin-mat@sust.edu (Md.A. Uddin)

widely used are either spectral method or the conventional finite difference method with structured grids. Among these two methods, the conventional finite difference method [8, 17] is the most straightforward one. For time integration or for temporal discretization of the governing equations of LES the low-storage explicit Runge-Kutta methods are a popular choice. The low-storage Runge-Kutta methods [11, 28] call for minimum levels of memory locations during the time integration and can easily adapt with the modern large-scale scientific computing needs.

Therefore, the objective of this study is to perform LES in a plane turbulent channel flow with near wall region approximation by AWM and DEWM. The spatial discretization of the governing equations of LES is done by a second order finite difference formulation, and for the temporal discretization a low-storage explicit Runge-Kutta method with third order accuracy is applied. For subgrid scale (SGS) modeling in LES the Standard Smagorinsky model (SSM) is used. Essential turbulence statistics based on these two LES approaches are calculated and compared with DNS data of Moser et al. [18]. Instantaneous streamwise shear velocity distribution at the immediate vicinity of the wall and instantaneous streamwise velocity distribution at the centerline plane of the channel are also computed from the two LES approaches and compared in different contour plots. Vortical structures in the computed flow field in 3D turbulent channel flow are visualized by iso-surfaces of second invariant of velocity gradient tensor. More specifically, the prime objective of this study is to compare the performance of AWM and DEWM in LES.

2. Governing Equations

The governing equations of LES for an incompressible plane turbulent channel flow are the filtered Navier-Stokes and continuity equations. In Cartesian co-ordinates these equations can be written as

$$\frac{\partial \bar{u}_i}{\partial t} + \frac{\partial}{\partial x_j}(\bar{u}_i.\bar{u}_j + \tau_{ij}) = -\frac{1}{\rho}\frac{\partial \bar{p}}{\partial x_i} + \frac{\partial}{\partial x_j}\left[\nu\left(\frac{\partial \bar{u}_i}{\partial x_j} + \frac{\partial \bar{u}_j}{\partial x_i}\right)\right]$$

$$\frac{\partial \bar{u}_i}{\partial x_i} = 0$$

where the index $i, j = 1, 2, 3$ refers to the x, y and z directions respectively. Associated to these directions, $\bar{u}_x, \bar{u}_y$ and $\bar{u}_z$ are the streamwise, wall normal and spanwise filtered velocity respectively. $\bar{p}$ is the filtered pressure, ρ represents the fluid density and ν denotes the kinematic viscosity of the flow. τ_{ij} is SGS Reynolds stress tensor, which is unresolved term and must be modeled. The equations are non-dimensionalized by the channel half-width δ, and the wall shear velocity u_τ. The Reynolds number of such a flow is therefore written as $Re_\tau = u_\tau \delta/\nu$. A schematic geometry of the plane channel flow and the co-ordinate system are shown in Figure 1.
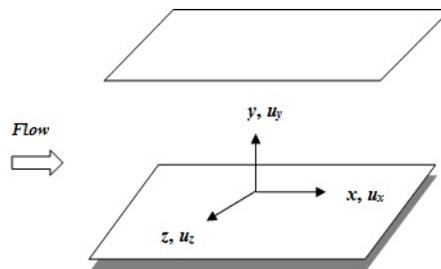

Figure 1. Schematic geometry of plane channel flow.

In LES, the velocity field u_i is decomposed into a filtered or large scale component $\bar{u}_i$ and a small or SGS component $\acute{u}_i$. This decomposition is done by applying a spatial filtering operation. Spatial filtering retains the large scale component to be resolved and remove the small scale component to be modeled. According to Sagaut [19], this decomposition is represented as:

$$u_i = \bar{u}_i + \acute{u}_i .$$

In this approach the effect of the SGS field appears through τ_{ij} , which is defined as

$$\tau_{ij} = \overline{u_i\, u_j} - \bar{u}_i\, \bar{u}_j.$$

Models used to approximate the τ_{ij} are called SGS models. Such a model represents the effect of the SGS field on the filtered filed. There are a number of SGS models. The most commonly used SGS model is the SSM [22]. According to this model, τ_{ij} is proportional to the local strain rate tensor of the filtered field, $\bar{S}_{ij}$ as follows:

$$\tau_{ij} = -2\,\nu_s\,\bar{S}_{ij}.$$

The proportionality factor is the SGS eddy viscosity, ν_s which is defined as

$$\nu_s = (C_s\,\Delta)^2|\bar{S}|.$$

The quantity C_s is the Smagorinsky constant, $\Delta = (\Delta x\,\Delta y\,\Delta z)^{1/3}$ is the size of the grid filter, and $|\bar{S}| = \sqrt{2\,\bar{S}_{ij}\,\bar{S}_{ij}}$ represents the magnitude of strain rate, where $\bar{S}_{ij} = \frac{1}{2}\left(\frac{\partial \bar{u}_i}{\partial x_j} + \frac{\partial \bar{u}_j}{\partial x_i}\right)$. In turbulent channel flow simulation the value of C_s in SSM is adjusted to improve the results. In this study we use the value of $C_s = 0.1$ and modify the SSM by introducing Van-Driest damping function, f_s [19] in ν_s as follows:

$$\nu_s = (C_s\,f_s\,\Delta)^2|\bar{S}|$$

in which $f_s = 1 - \exp\left(-\frac{y^+}{A^+}\right)$ is long been used to reduce the growth of small scales near the wall, where $A^+ = 25$ and y^+ is the distance from the wall in viscous wall units.

3. Grid System and Numerical Methods

In this numerical simulation, the spatial discretization is performed by staggered grid system and the coordinate system is the three dimensional Cartesian. In the staggered grid system, each independent variable is computed in different locations. This type of grid was introduced by Harlow and Welch [9] in constructing Marker-and-cell (MAC) method for pressure correction. Staggered grids may be constructed by several methods. An example of a staggered grid system in a two-dimensional plane is shown in our previous papers [15, 25].

When the computational domain is discretized by the grid points, the governing equations can be discretized in this domain for numerical solution. In this simulation, the governing equations are discretized in space by using the finite difference formulation with the second order accuracy and for discretization in time, a low-storage explicit Runge-Kutta method with the third order accuracy [11] is used. The spatial and temporal discretization methods are shortly described in our previous papers [15, 25]. The coupling between continuity equation and pressure fields is performed by the simplified marker-and-cell (SMAC) method [10]. Poisson equation for pressure is solved iteratively by a Preconditioned Incomplete Cholesky Decomposition Conjugated Gradient method.

4. Computational Parameters

The computational domain is $2\pi\delta\times2\delta\times\pi\delta$ and the domain is discretized by $32\times20\times32$ grid points in the streamwise, wall normal and spanwise directions, respectively. The grid spacings in the corresponding directions are uniform which are $\Delta x^+ \approx 116$, $\Delta y^+ \approx 59$ and $\Delta z^+ \approx 58$ wall units respectively. The superscript $'+'$ indicates a non-dimensional quantity scaled by the wall variables; e.g. $y^+ = yu_\tau/\nu$. A sample of grid generation in the given domain is shown in Figure 2. The simulation is performed at a Reynolds number $Re_\tau = 590$ which is based on δ and u_τ. The computation is carried out with a non-dimensional time increment, $\Delta t = 0.002$, which maintained CFL numbers [14, 15, 25] 0.325 and 0.330 for LES-AWM and LES-DEWM approaches respectively. The CFL number is defined as

$$CFL = \Delta t\,\max\left(\frac{|\langle\bar{u}_x\rangle|}{\Delta x} + \frac{|\langle\bar{u}_y\rangle|}{\Delta y} + \frac{|\langle\bar{u}_z\rangle|}{\Delta z}\right)$$

where $\langle\bar{u}_i\rangle$ represents an ensemble average of $\bar{u}_i$. To get the fully resolved scales of turbulence the computation is executed up to time, $t = n\,\Delta t$, where n is the number of time step.

5. Wall Models

In the LES calculation, the first off-wall grid points are at $y^+ \approx 29.5$ wall unit. In this study, in the LES-AWM and LES-DEWM approaches the region in between the first off-wall grid points in LES and the wall is approximated by AWM and DEWM respectively which are shortly described below.
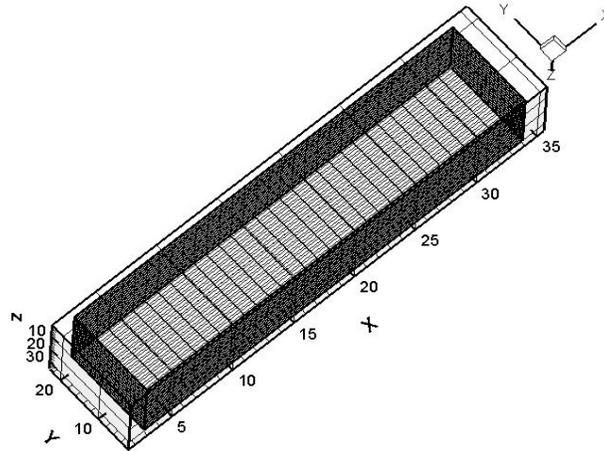
FIGURE 2. A sample of grid generation in the plane channel.

5.1. **AWM.** This model is given by Spalding [23]. In this model, the wall shear stresses are calculated using Spalding's law of which the special form is

$$y^+ = f(u^+) = u^+ + A\left[\exp(\kappa u^+) - 1 - (\kappa u^+)/2 - (\kappa u^+)^3/6 - (\kappa u^+)^4/24\right] \tag{5.1}$$

where, $A = \exp(-\kappa B) = 0.1108$, $\kappa = 0.4$ and $B = 5.5$. In this equation, $y^+ = y u_\tau / \nu$ where y is the distance from the wall, and $u^+ = u/u_\tau$ is the non-dimensional velocity at the first off-wall computational cells where u is the instantaneous horizontal velocity.

At the wall the Spalding's law satisfies the no-slip condition and at the first off-wall grid points the LES velocity, $\sqrt{\langle \bar{u}_x \rangle^2 + \langle \bar{u}_z \rangle^2}$ is substituted to u in equation (5.1). Then this equation is solved by Newton Raphson method for u_τ which is used to calculate the instantaneous wall shear stresses:

$$\tau_{w,x/\rho} = (\nu y^+/u^+)\bar{u}_x\,y,\ \tau_{w,z/\rho} = (\nu y^+/u^+)\bar{u}_z\,y.$$

These wall shear stress components are then used as the approximate wall boundary conditions of velocity fields in the LES-AWM approach.

5.2. **DEWM.** In this model, the unsteady thin boundary layer equations are solved numerically at the near wall region. The governing equations of this model for horizontal velocity components U_i ($i = 1, 3$) are [4, 27]:

$$\frac{\partial U_i}{\partial t} + \frac{\partial (U_i.U_j)}{\partial x_j} = -\frac{\partial P}{\partial x_i} + \frac{\partial}{\partial x_2}\left[(\nu + \nu_T)\frac{\partial U_i}{\partial x_2}\right]$$

with continuity

$$U_2 = -\int_0^{x_2}\left(\frac{\partial U_1}{\partial x_1} + \frac{\partial U_3}{\partial x_3}\right)dx_2.$$

In these equations, the index 1, 2, 3 refers to the streamwise, wall normal and spanwise directions respectively. The pressure P, which is assumed to be x_2 - independent and equated to the values from the outer-flow LES calculation. ν_T is the turbulent eddy viscosity which is achieved from a RANS type mixing-length eddy viscosity model with near-wall damping [3, 4, 27]:

$$\frac{\nu_T}{\nu} = \kappa\, y_w^+\left(1 - e^{-y_w^+/A}\right)^2.$$

In this mixing-length model $y_w^+ = \frac{y_w u_\tau}{\nu}$ is the distance from the wall in wall units, κ is the model co-efficient, and A is a constant which is 19. At the first off-wall computational cells the values of horizontal velocity components are

obtained from the outer-flow LES velocity nodes and the wall boundary condition is no-slip. With these boundary conditions, the governing equations are solved by using the second order Adams-Bashforth scheme in time and the finite difference formulae in space of second order accuracy. The solutions are then used to determine the wall shear stresses, τ_{wi} ($i = 1, 3$) from the wall gradient:

$$\tau_{wi} = \nu \left. \frac{\partial U_i}{\partial x_2} \right|_{x_2=0}.$$

These wall shear stresses are then used as the approximate wall boundary conditions of velocity fields in the LES-DEWM approach.

6. Initial and Boundary Conditions

In this simulation the initial flow field is the random solenoidal velocity field. Many flows that have been studied by DNS and LES approximations have one or more directions of homogeneity that allow the application of periodic boundary conditions. Periodic boundary conditions are easy to implement and efficient. In this study, periodic boundary conditions are applied in the streamwise and spanwise directions and the wall boundary condition is no-slip. In the staggered arrangement, additional nodes are set up surrounding the physical boundaries. The computations are done at the interior nodes only. Just outside the solution domain the values of the velocity components are equated to the values of the nearest node just inside the solution domain [26]. For the scalar variable pressure, the periodic boundary conditions are used in the streamwise and spanwise directions. In the wall normal direction just outside the solution domain the values of pressure are determined by assuming a zero gradient [1].

7. Results and Discussions

7.1. **Turbulence Statistics.** In this section we calculate some essential turbulence statistics from the computed flow fields of the two LES approximations in 3D turbulent channel flow. The statistical results are shown in the lower half of the channel. In order to verify the performance of the two LES approaches the statistical results are compared with DNS data of Moser et al. [18]. For comparison, the DNS data obtained by Moser et al. [18] is represented by a solid line, LES results using AWM by a dashed line, LES results using DEWM in between the wall and first off-wall grid points in LES by a dotted line and the results in rest of the region for this approach are indicated by a dashed dot dot line. The statistical results trace the data throughout the calculation domain. In a plane turbulent channel flow this domain can be divided into two parts. One is the inner or near wall region and the other is the outer region. Each of these regions is split into several layers corresponding to different types of dynamics. In the inner region the dynamics is dominated by viscous effects, and in the outer region it is controlled by turbulence. For canonical boundary layer case, the inner region can be subdivided into three layers: viscous sub-layer ($y^+ \leq 5$), buffer layer ($5 < y^+ \leq 30$) and logarithmic inertial layer ($y^+ > 30$; $y/\delta \ll 1$) [19]. The outer region consists of the end of the logarithmic inertial layer and wake region.

The profiles of mean velocity normalized by the wall-shear velocity corresponding to the lower half of the channel from the LES-AWM and LES-DEWM approaches are shown in Figure 3. The mean velocity is calculated by

$$u_x^+ = \frac{\langle \bar{u}_x \rangle}{u_\tau}.$$

A circle located at about $y^+ \approx 30.0$ in this figure specifies the interface between the RANS and LES regions. That is, in the LES approximation based on DEWM the RANS region is defined as the viscous sub-layer and the buffer layer. Rest of the region can be termed as the LES region. In this figure it can be observed that the LES profile based on AWM cannot trace data in the whole boundary layer, whereas the LES profile based on DEWM can resolve the whole boundary layer. In the RANS region, within the viscous sub-layer the LES profile based on DEWM is almost collapsed with the DNS profile, hereafter in the buffer layer the LES profile under predicts the DNS profile. In the LES region, from $y^+ \approx 30.0$ to $y^+ \approx 80.0$ the LES profile based on DEWM under predicts the DNS profile, but in rest of the region there is hardly noticeable difference between the two profiles. On the other hand, the LES profile based on AWM starts from $y^+ \approx 30.0$. Initially, from $y^+ \approx 30.0$ to $y^+ \approx 40.0$ the LES-AWM profile under predicts the DNS profile, hereafter in rest of the region the LES-AWM profile is seen to be over predicted. Nonetheless, Figure 3 shows that the agreement of the mean velocity profile for the LES-DEWM approach with the DNS data is better than that of the LES-AWM approach.
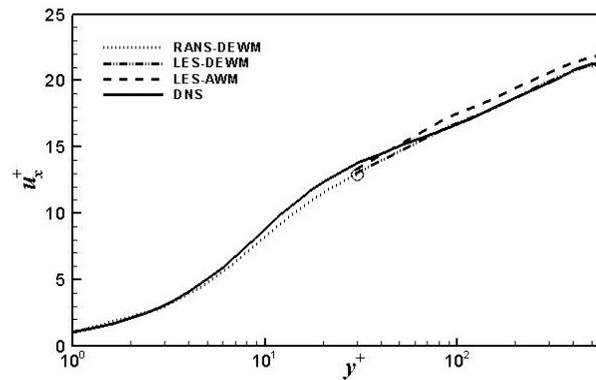
FIGURE 3. The mean velocity profile in wall units.

TABLE 1. Comparison between the results of mean velocity in LES region for different approximations

y^+	DNS	LES-AWM	LES-DEWM
31.06	13.88	13.35	13.05
41.00	14.49	14.49	14.00
88.50	16.43	17.22	16.47
165.42	18.00	18.65	18.00
230.74	19.09	19.90	19.11
327.44	20.13	20.81	20.15
370.33	20.59	21.20	20.59
501.50	21.10	21.79	21.05

Table 1 provides a sample of the quantitative comparison between the results of the mean velocity at some positions of the channel obtained from different simulation approaches. In this comparison the DNS data are let as the true value since DNS is considered as the exact approach to turbulence simulation. From this table one can easily calculate the percentage of relative errors generated in the LES data at the corresponding positions. As for example, at the position $y^+ \approx 31.06$ the percentage of relative error in the LES result for the LES-DEWM approach is 5.98%. After this position, the error decreases for this approach and at the position $y^+ \approx 165.42$ it becomes zero. Then, again the discrimination between the results of the DNS and LES-DEWM approaches are observed and at the position $y^+ \approx 370.33$ there is no separation between the DNS and LES data. On the other hand, for the LES-AWM approach the relative error generated in this profile at the position $y^+ \approx 31.06$ is 3.82%. After this position, the separation between the DNS and LES results decreases and at $y^+ \approx 41.00$ the relative error appears to zero. Then, again the discriminations between the two results are observed. After all, it is worth noting here that the errors generated in this profile for the LES-DEWM approach are smaller than that for the LES-AWM approach at maximum positions.

Figures 4(a, b, c) show the DNS and LES profiles of normalized root mean square (r.m.s.) velocity components corresponding to the lower half of the channel. The root mean square velocity components are normalized by the wall shear velocity which are defined as:

$$u^+_{x\,r.m.s} = \sqrt{\langle \bar{u}_x^2 \rangle - \langle \bar{u}_x \rangle^2} \Big/ u_\tau$$

$$u^+_{y\,r.m.s} = \sqrt{\langle \bar{u}_y^2 \rangle - \langle \bar{u}_y \rangle^2} \Big/ u_\tau$$

$$u^+_{z\,r.m.s} = \sqrt{\langle \bar{u}_z^2 \rangle - \langle \bar{u}_z \rangle^2} \Big/ u_\tau \, .$$

From these three figures it can be observed that although there exists a noticeable discrepancy between the LES profiles near the wall position ($0 < y^+ < 100$), but after this position in rest of the domain there is hardly noticeable difference
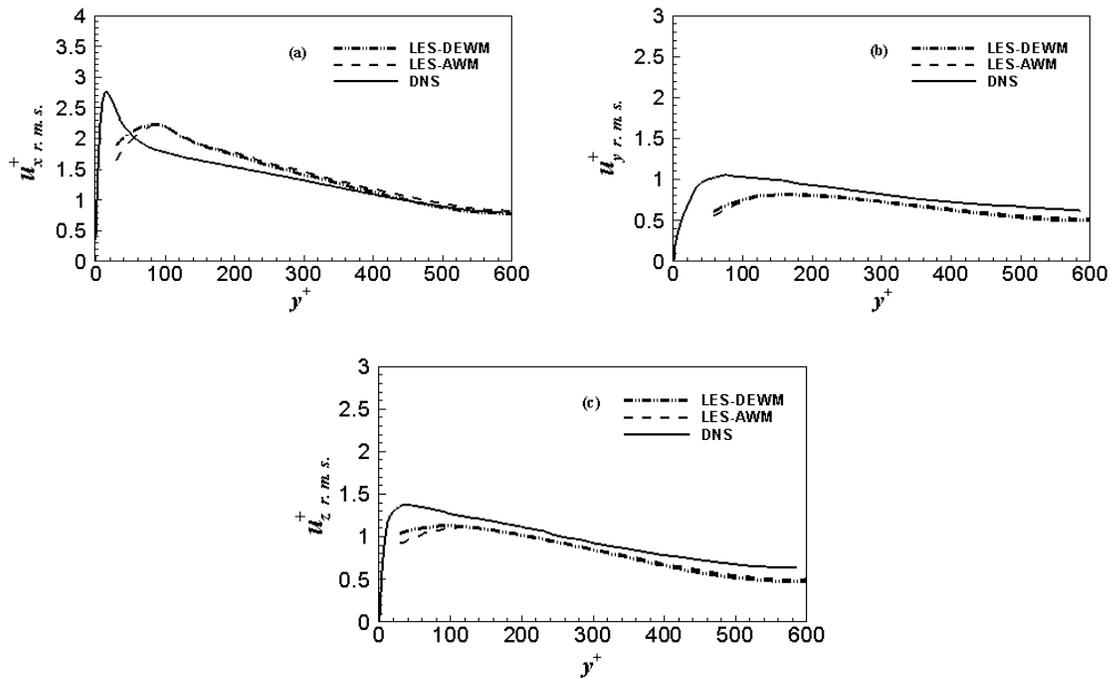
FIGURE 4. Root mean square velocity profiles in wall units.

between these two LES profiles. In comparison with the DNS profile, it has to be noted that in Figure 4(a) the LES profiles over predict the DNS profile almost in the whole range. But, beyond $y^+ \approx 400$ the LES-DEWM profile is almost collapsed with the DNS profile. In the Figures 4(b) and 4(c), the LES profiles under predict the DNS profile in the whole calculation range. Moreover, in these three figures it is important to note that the LES-DEWM profiles show closer agreement with the DNS profile than that of the LES-AWM profiles.
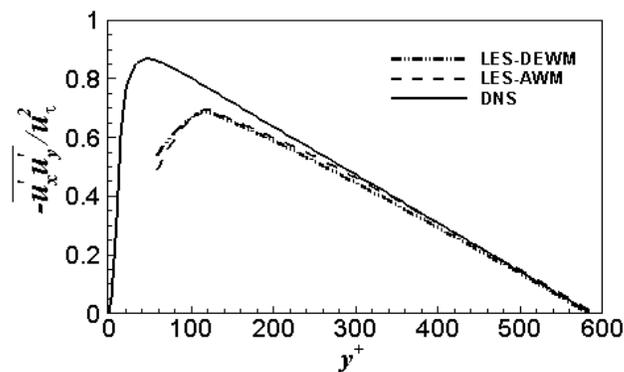

FIGURE 5. The Reynolds stress profile in wall units.

Figure 5 represents the profiles of non-dimensional Reynolds stress, $-\frac{\overline{\hat{u}_x \hat{u}_y}}{u_\tau^2}$ for different approximations in the lower half of the channel. In a fully developed channel flow at an equilibrium state this profile appears to a straight line. From this figure it can be observed that although there exists a noticeable discrepancy between the DNS and LES results at

the near wall region but away from the wall our computed profiles appear to a straight line which are close and similar to DNS profile.

7.2. **Flow Structures.** In this section we discuss about the flow structures in the computed flow field obtained from the two LES approximations by different contour plots and iso-surfaces. To compare the flow structures from the LES-AWM and LES-DEWM approaches we have calculated streamwise velocity ($\bar{u}_x$) distribution at the centerline plane of the channel and streamwise shear velocity ($\bar{u}_{x\tau}$) distribution at the immediate vicinity of the wall. We also show the vortical structures in the 3D turbulent channel flow by iso-surfaces of the second invariant Q of velocity gradient tensor.
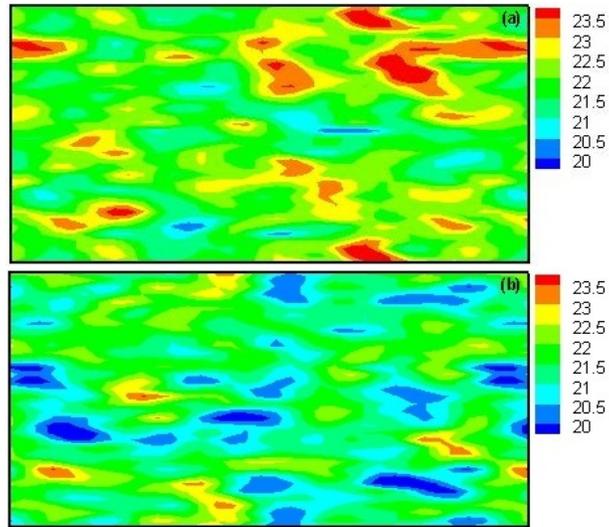

FIGURE 6. Contours of $\bar{u}_x$ profiles in x-z plane for (a) LES-AWM, and (b) LES-DEWM approaches.

Contours of instantaneous $\bar{u}_x$ distributions at the centerline $x - z$ plane of the channel for the LES-AWM and LES-DEWM approaches are shown in Figures 6(a, b). The distributions have been collected at the end time of calculation. In these contour plots the values of $\bar{u}_x$ ranged between 20 and 23.5. The lowest value appears at blue regions, while the highest value at red regions. The larger values of $\bar{u}_x$ appear more densely in Figure 6(a) than that in Figure 6(b). On the other hand, the smaller values of $\bar{u}_x$ are more located in Figure 6(b) than that in Figure 6(a). In both of the figures the appearance of the regions of medium values of $\bar{u}_x$ are significant.

Contours of instantaneous $\bar{u}_{x\tau}$ distribution at the immediate vicinity of the wall of this channel in $x - z$ plane for the two LES approximations are displayed in Figures 7(a, b). $\bar{u}_{x\tau}$ can be calculated from equation (7.1):

$$\bar{u}_{x\tau} = \sqrt{\frac{\tau_x}{\rho}} \tag{7.1}$$

where, $\bar{u}_{x\tau}$ = streamwise shear velocity
ρ = density of the fluid
τ_x = streamwise shear stress.
In these contour plots the values of $\bar{u}_{x\tau}$ ranged between 0.8 and 1.4. The lowest value is indicated by a blue color, while the highest value by a red color. The results in Figure 7(a) are from the LES-AWM approach and the results in Figure 7(b) are from the LES-DEWM approach. From these contour plots it can be observed that the regions of lowest and highest value of $\bar{u}_{x\tau}$ appear more densely for the LES-DEWM approach than that of the LES-AWM approach. It is also noticeable that the larger values of $\bar{u}_{x\tau}$ appear at scattered locations in the whole distribution for both the LES approximations and the existence of the regions of medium values are more located in Figure 7(a) than that in Figure 7(b).
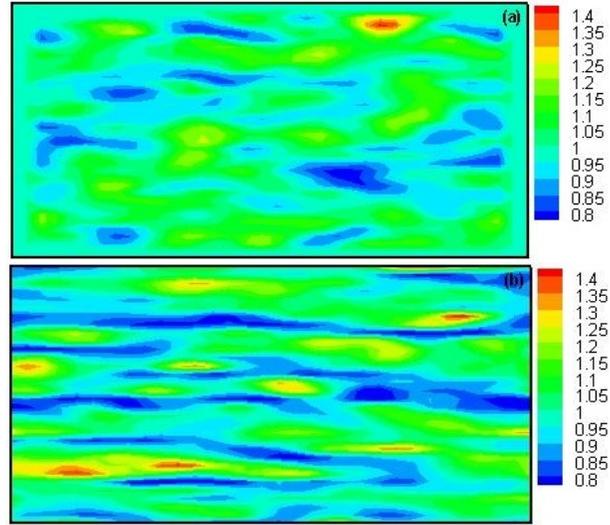
FIGURE 7. Contours of $u^-_{x\tau}$ profiles in x-z plane for (a) LES-AWM, and (b) LES-DEWM approaches.

Figures 8(a, b) represent the visualization of vortical structures in the 3D turbulent channel flow for the two LES approximations. The vortices are visualized by iso-surfaces of the second invariant of velocity gradient tensor. The second invariant, Q is defined as [24]:

$$Q = -\frac{1}{2}\Big(S_{ij}\, S_{ij} - \Omega_{ij}\, \Omega_{ij}\Big) \tag{7.2}$$

where,

$$S_{ij} = \frac{1}{2}\Big(\frac{\partial \bar{u}_i}{\partial x_j} + \frac{\partial \bar{u}_j}{\partial x_i}\Big) \text{ and } \Omega_{ij} = \frac{1}{2}\Big(\frac{\partial \bar{u}_i}{\partial x_j} - \frac{\partial \bar{u}_j}{\partial x_i}\Big).$$

These S_{ij} and Ω_{ij} are the strain-rate and rotation tensors respectively, which are the symmetric and asymmetric part of the velocity gradient tensor:

$$A_{ij} = \frac{\partial u_i}{\partial x_j} = S_{ij} + \Omega_{ij}.$$

The velocity gradient tensor represents the balance between the rotation and strain rate tensors. Flow visualization based on this velocity gradient tensor links the inner and outer regions of the turbulent flow field. In these figures, the flow visualized region is the whole calculation domain. In Figure 8(a) the near wall region is approximated by AWM, and Figure 8(b) is obtained from the LES-DEWM approach. In the both figures the iso-surfaces are at value $Q = 5$. For this value of Q the vortical structures are significant. It is also noticeable that for both the LES approaches the vortices are distributed randomly over the turbulent flow field. The vortices are generated more densely near the boundary of the channel than that of around the central position of the channel.

8. CONCLUSIONS

A Large eddy Simulation of a plane turbulent channel flow has been performed successfully with near wall region approximation by AWM and DEWM. The simulation has been carried out with $32 \times 20 \times 32$ grid points at a Reynolds number, 590 which is based on the channel half width and wall shear velocity. With the low resolution the simulations enabled to resolve the essential features of the statistical fields. The LES approximation based on DEWM can resolve the whole boundary layer. On the other hand, the LES approximation based on AWM cannot trace the data in the whole boundary layer. The LES with DEWM can capture the effects of near wall structures more accurately than that of the LES with AWM. The LES approach with AWM can reduce the computational cost more than that of the LES approach with DEWM. In agreement with the DNS data, the LES results based on DEWM show better agreement than that of the LES results based on AWM. Instantaneous streamwise velocity distribution at the centerline xz–plane and instantaneous streamwise shear velocity distribution at the immediate vicinity of the wall of this channel have
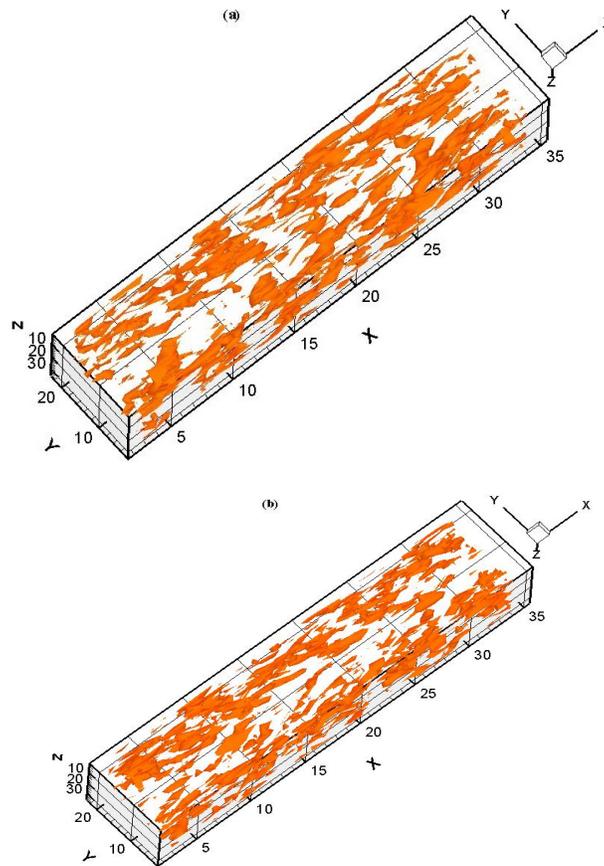
FIGURE 8. Iso-surfaces of the second invariant ($Q = 5$) in the channel flow for (a) LES-AWM, and (b) LES-DEWM approaches.

also been measured in the contour plots for both the LES approaches. In these contour plots, one of the distinctive features in streamwise velocity distributions is that the existence of the regions of larger values of streamwise velocity are more located for the LES-AWM approach than that for LES-DEWM. In the streamwise shear velocity distributions the lowest and highest values appear more densely for the LES-DEWM approach than that for LES-AWM. Vortical structures in the computed flow field for both the LES approaches are visualized by iso-surfaces of the second invariant of velocity gradient tensor. For both the approaches the vortices are distributed randomly over the turbulent flow field and generated more densely near the boundary of the channel.

REFERENCES

[1] Anderson, Jr. J. D., Computational Fluid Dynamics, McGraw-Hill, New York, 1995. 6

[2] Balaras, E., Benocci, C., Piomelli, U., *Two-layer approximate boundary conditions for large-eddy simulations*, AIAA J., **34(6)**(1996), 1111-1119. 1

[3] Cabot, W., *Large-Eddy Simulations with Wall Models*, In: Annual Research Briefs 1995, Center for Turbulence Research, Stanford University, CA, 1995, 41-50. 1, 5.2

[4] Cabot, W., Moin, P., *Approximate Wall Boundary Conditions in the Large-Eddy Simulation of High Reynolds Number Flow*, J. Flow Turbulence Combust., **63**(2000), 269-291. 1, 5.2

[5] Dritselis, C. D., *Large eddy simulation of turbulent channel flow with transverse roughness elements on one wall*, Int. J. Heat Fluid Flow, **50**(2014), 225-239. 1

[6] Ferziger, J. H., Peric´, M., Computational Methods for Fluid Dynamics, Springer-Verlag, Berlin, 2002. 1

[7] Grötzbach, G., *Direct numerical and large eddy simulation of turbulent channel flows*, In: Encyclopedia of Fluid Mechanics 1987, Cheremisinoff, NP ed: Gulf Pub, Chap. 34, 1987, 1337-1391. 1

[8] Ham, F. E., Lien, F. S., Strong, A. B., *A Fully Conservative Second-Order Finite Difference Scheme for Incompressible Flow on Nonuniform Grids*, J. Comput. Phys., **177**(2002), 117-133. 1

[9] Harlow, F. H., Welch, J. E., *Numerical calculation of time-dependent viscous incompressible flow with free surface*, Phys. Fluids, **8(12)**(1965), 2182-2189. 3

[10] Johnson, D. B., Raad, P. E., Chen, S., *Simulation of impacts of fluid free surfaces with solid boundaries*, Int. J. Numer. Methods Fluids, **19(2)**(1994), 153-176. 3

[11] Kennedy, C. A., Carpenter, M. H., Lewis, R. M., *Low-storage, explicit Runge-Kutta schemes for the compressible Navier-Stokes equations*, Appl. Numer. Math., **35**(2000), 177-219. 1, 3

[12] Kianejad, S. S., Ansarifard, N., *Numerical Simulation of Turbulent Boundary Layers of Surfaces Covered with Foul Release and Antifouling Coatings*, J. Nav. Arch. Marine Eng., **13**(2016), 17-26. 1

[13] Kim, J., Moin, P., Moser, R., *Turbulence statistics in fully developed channel flow at low Reynolds number*, J. Fluid Mech., **177**(1987), 133-166. 1

[14] Mallik, M. S. I., Uddin, M. A., *Large Eddy Simulation of Turbulent Channel Flow using Algebraic Wall Model*, J. Kor. Soc. Ind. Appl. Math., **20(1)**(2016), 37-50. 1, 4

[15] Mallik, M. S. I., Uddin, M. A., Meah, M. A., *Large Eddy Simulation of Turbulent Channel Flow at Re_τ = 590*, IOSR J. Math., **10(6)**(2014), 41-50. 1, 3, 4

[16] Mallik, M. S. I., Uddin, M. A.,Rahman, M. A., *Direct Numerical Simulation in Two Dimensional Homogeneous Isotropic Turbulence using Spectral Method*, J. Sci. Res., **5(3)**(2013), 435-445. 1

[17] Morinishi, Y., *Skew-symmetric form of convective terms and fully conservative finite difference schemes for variable density low-Mach number flows*, J. Comput. Phys., **229**(2010), 276-300. 1

[18] Moser, R. D., Kim, J., Mansour, N. N., *Direct numrical simulation of turbulent channel flow up to Re_τ = 590*, Phys. Fluids, **11(4)**(1999), 943-945. 1, 7.1

[19] Sagaut, P., Large Eddy Simulation for Incompressible Flows: An Introduction, Springer-Verlag, Berlin, 2001. 1, 2, 7.1

[20] Sanderse, B., Koren, B., *Accuracy analysis of explicit Runge-Kutta methods applied to the incompressible Navier-Stokes equations*, J. Comput. Phys., **231(8)**(2012), 3041-3063.

[21] Schumann, U., *Subgrid scale model for finite difference simulations of turbulent flows in plane channels and annuli*, J. Comput. Phys., **18**(1975), 376-404. 1

[22] Smagorinsky, J., *General circulation experiments with the primitive equations*, I: The basic experiment, Mon. Weather Rev., **91(3)**(1963), 99-165. 2

[23] Spalding, D. B., *A single formula for the law of the wall*, J. Appl. Mech., **28(3), Ser. E**(1961), 455-458. 1, 5.1

[24] Uddin, A., Kato, C., Yamade, Y., Ohshima, N., Tanahashi, M., Miyauchi, T., *Large Eddy Simulation of Homogeneous Isotropic Turbulent Flow using the Finite Element Method*, JSME Int. J., **49(1), Ser. B**(2006), 102-114. 1, 7.2

[25] Uddin, M. A., Mallik, M. S. I., *Large Eddy Simulation of Turbulent Channel Flow using Smagorinsky Model and Effects of Smagorinsky Constants*, Brit. J. Math. Comp. Sci., **7(5)**(2015), 375-390. 1, 3, 4

[26] Versteeg, H. K., Malalasekera, W., An introduction to computational fluid dynamics, Longman Group Limited, England, 1995. 6

[27] Wang, M. P., Moin, P., *Dynamic wall modeling for large-eddy simulation of complex turbulent flows*, Phys. Fluids, **14(7)**(2002), 2043-2051. 1, 5.2

[28] Williamson, J. H., *Low-storage Runge-Kutta schemes*, J. Comput. Phys., **35**(1980), 48-56. 1

[29] Xie, Z., Lin, B., Falconer, R. A., *Large-eddy simulation of the turbulent structure in compound open-channel flows*, Adv. Water Resour., **53**(2013), 66-75. 1

[30] Yang, F., Zhang, H. Q., Chan, C. K., Wang, X. L., *Large Eddy Simulation of Turbulent Channel Flow with 3D Roughness Using a Roughness Element Model*, Chinese Phys. Lett., **25(1)**(2008), 191-194. 1